Evidence for a dynamical ground state in the frustrated pyrohafnate $Tb_2Hf_2O_7$

V. K. Anand,[1,*] L. Opherden,[2,3] J. Xu,[1] D. T. Adroja,[4,5] A. D. Hillier,[4] P. K. Biswas,[4] T. Herrmannsdörfer,[2] M. Uhlarz,[2] J. Hornung,[2,3] J. Wosnitza,[2,3] E. Canévet,[6,7] and B. Lake[1,†]

[1]*Helmholtz-Zentrum Berlin für Materialien und Energie GmbH, Hahn-Meitner Platz 1, D-14109 Berlin, Germany*
[2]*Dresden High Magnetic Field Laboratory (HLD-EMFL), Helmholtz-Zentrum Dresden-Rossendorf, 01328 Dresden, Germany*
[3]*Institut für Festkörper- und Materialphysik, TU Dresden, 01062 Dresden, Germany*
[4]*ISIS Facility, Rutherford Appleton Laboratory, Chilton, Didcot, Oxon OX11 0QX, United Kingdom*
[5]*Highly Correlated Matter Research Group, Physics Department, University of Johannesburg,*
P.O. Box 524, Auckland Park 2006, South Africa
[6]*Laboratory for Neutron Scattering and Imaging, Paul Scherrer Institute, CH-5232 Villigen PSI, Switzerland*
[7]*Department of Physics, Technical University of Denmark, 2800 Kgs. Lyngby, Denmark*

We report the physical properties of $Tb_2Hf_2O_7$ based on ac magnetic susceptibility $\chi_{ac}(T)$, dc magnetic susceptibility $\chi(T)$, isothermal magnetization $M(H)$, and heat capacity $C_p(T)$ measurements combined with muon spin relaxation (μSR) and neutron powder diffraction measurements. No evidence for long-range magnetic order is found down to 0.1 K. However, $\chi_{ac}(T)$ data present a frequency-dependent broad peak (near 0.9 K at 16 Hz) indicating slow spin dynamics. The slow spin dynamics is further evidenced from the μSR data (characterized by a stretched exponential behavior) which show persistent spin fluctuations down to 0.3 K. The neutron powder diffraction data collected at 0.1 K show a broad peak of magnetic origin (diffuse scattering) but no magnetic Bragg peaks. The analysis of the diffuse scattering data reveals a dominant antiferromagnetic interaction in agreement with the negative Weiss temperature. The absence of long-range magnetic order and the presence of slow spin dynamics and persistent spin fluctuations together reflect a dynamical ground state in $Tb_2Hf_2O_7$.

I. INTRODUCTION

The discovery of spin-ice behavior in $Dy_2Ti_2O_7$ and $Ho_2Ti_2O_7$ and associated magnetic monopole dynamics have created a great research interest in the rare-earth pyrochlore oxides $R_2B_2O_7$ (R is a trivalent rare-earth ion and B a tetravalent transition-metal ion or Ge, Sn, Pb) [1–10]. These materials contain corner-sharing tetrahedra of R^{3+} ions which provide a very suitable condition for realizing frustrated magnetism. With this atomic arrangement, the interplay of crystal electric field (CEF), antiferromagnetic exchange, and ferromagnetic dipolar interactions lead to diverse magnetic states in these materials [1]. The spin-ice state is realized with the frustrated "two-in/two-out" spin configuration resulting from ferromagnetic interactions with local $\langle 111 \rangle$ Ising anisotropy [4]. On the other hand, antiferromagnetic interactions result in an "all-in/all-out" spin configuration [11–15]. Spin-liquid behavior is another interesting magnetic ground state that has been observed in $Tb_2Ti_2O_7$ [1,2].

$Tb_2Ti_2O_7$, like the spin-ice compounds $Dy_2Ti_2O_7$ and $Ho_2Ti_2O_7$, also has a CEF-split doublet ground state and displays $\langle 111 \rangle$ Ising anisotropy. Despite a large negative Weiss temperature ($\theta_p = -19$ K), no signature of long-range magnetic order has been found in $Tb_2Ti_2O_7$ down to 50 mK [16–19]. As the effective interaction in $Tb_2Ti_2O_7$ is anti-ferromagnetic in nature, the $\langle 111 \rangle$ anisotropy should not cause magnetic frustration; accordingly, a long-range ordered magnetic ground state is expected. In order to explain the low-temperature properties of $Tb_2Ti_2O_7$, two theoretical scenarios have been proposed: (a) a quantum spin-ice (QSI) scenario [20,21], and (b) a nonmagnetic singlet ground-state scenario [22]. In the QSI scenario, virtual quantum excitations between the CEF ground-state doublet and the first excited doublet ($\sim$15 K) have been proposed to renormalize the effective low-energy spin Hamiltonian such that the ground state of $Tb_2Ti_2O_7$ is a quantum spin-ice state [20,21]. The second scenario argues that $Tb_2Ti_2O_7$ undergoes a Jahn-Teller transition leading to a singlet ground state with a sufficiently large splitting between ground state and first excited state which prevents long-range order [22]. Recent neutron scattering investigations on $Tb_2Ti_2O_7$ have been reported to show evidence for pinch points and Coulomb correlations which favor the QSI picture [23–27].

The intriguing magnetic ground state of $Tb_2Ti_2O_7$ motivated us to investigate the Hf analog of this compound, namely, $Tb_2Hf_2O_7$. Recently, we investigated the physical properties of the hafnate pyrochlores $Nd_2Hf_2O_7$ [15,28] and $Pr_2Hf_2O_7$ [29]. $Nd_2Hf_2O_7$ was found to exhibit a long-range antiferromagnetic order below $T_N \approx 0.55$ K for which our neutron diffraction study revealed an all-in/all-out arrangement of Nd^{3+} moments [15]. Inelastic neutron scattering confirmed the Ising anisotropy of $Nd_2Hf_2O_7$ with a Kramers doublet ground state of dipolar-octupolar character [28]. Interestingly, muon spin relaxation (μSR) revealed the presence of

*vivekkranand@gmail.com
†bella.lake@helmholtz-berlin.de

persistent dynamic spin fluctuations deep inside the ordered state because of which the magnetic moment in the ordered state [$0.62(1)\mu_B$/Nd at 0.1 K] is strongly reduced [15,28]. On the other hand, $Pr_2Hf_2O_7$ with a non-Kramers doublet ground state is found not to show long-range magnetic order down to 90 mK, although slow spin dynamics and spin freezing are inferred from ac magnetic susceptibility data [29]. The magnetic ground state of $Pr_2Hf_2O_7$ possesses the ingredients for quantum spin-ice behavior [29,30].

Extending our work on hafnate pyrochlores, here we present physical properties of $Tb_2Hf_2O_7$. The magnetic ion Tb^{3+} ($4f^8$, $S = 3$, $L = 3$, $J = 6$) is a non-Kramers ion. The ($2J + 1 = 13$)-fold degenerate free-ion ground-state multiplet $^7F_6$ of Tb^{3+}, when subject to crystal field in the cubic pyrochlore structure, splits into four doublets and five singlets. Structural characterizations on $Tb_2Hf_2O_7$ report the presence of disorder (defect fluorite) in the pyrochlore structure of this compound [31]. The presence of structural disorder can perturb the crystal-field environment which in turn can modify the CEF states (splitting energies and levels scheme) which have a strong bearing on the magnetic ground state of such systems. The magnetic ground states of the pyrochlores $Tb_2Ti_2O_7$ and $Tb_2Sn_2O_7$ differ significantly, likely on account of the difference in their CEF states [32].

Our μSR study on $Tb_2Hf_2O_7$ shows the absence of long-range magnetic order down to 0.3 K; however, persistent spin fluctuations and slow spin dynamics are inferred from the μSR data. The ac magnetic susceptibility shows a frequency-dependent broad peak which also reflects a slow spin dynamics in $Tb_2Hf_2O_7$. Consistent with μSR and ac susceptibility data, the neutron powder diffraction data also suggest the absence of long-range magnetic order. The absence of magnetic ordering and presence of persistent spin fluctuations suggest a dynamical ground state in $Tb_2Hf_2O_7$. A recent work by Sibille *et al.* [33] reports a Coulomb spin-liquid behavior in this compound.

II. EXPERIMENTAL DETAILS

Polycrystalline $Tb_2Hf_2O_7$ was prepared at the Core Lab for Quantum Materials, Helmholtz-Zentrum Berlin (HZB) by solid-state reaction similar to the synthesis of pyrohafnates $Nd_2Hf_2O_7$ [15] and $Pr_2Hf_2O_7$ [29]. High-purity Tb_2O_3 (99.99%) and HfO_2 (99.95%), taken in stoichiometric ratio, were mixed and ground properly and fired at 1300 °C for 50 h followed by three additional successive grindings, pelletizings, and firings at 1400 °C, 1500 °C, and 1550 °C for 80 h each. The sample quality and crystallographic parameters were checked by room-temperature x-ray powder diffraction (XRD). The XRD data were refined using the software FULLPROF [34].

The dynamic (ac) susceptibility was measured using a noncompensated coil connected to an LR700 (16 Hz) or a lock-in amplifier (333 Hz–44.4 kHz) at Helmholtz-Zentrum Dresden-Rossendorf. The sample was precooled to 2 K using a physical property measurement system (PPMS) and further cooled by adiabatic demagnetization of a paramagnetic salt.

The dc susceptibility and isothermal magnetization measurements in the temperature range 2–300 K and with magnetic fields up to 14 T were made using a vibrating sample magnetometer (VSM) option of a Quantum Design PPMS at

the Core Lab for Quantum Materials, HZB. The heat capacity measurements between 1.8 and 300 K were performed by the adiabatic-relaxation technique using the PPMS at the Core Lab for Quantum Materials, HZB. The resistance measurement using a multimeter and resistivity option of PPMS indicated an insulating ground state for $Tb_2Hf_2O_7$.

The neutron powder diffraction (ND) measurements were performed on the cold neutron diffractometer DMC at Paul Scherrer Institute, Switzerland. The powder sample was mounted using a thin-walled copper can of diameter 10 mm. The sample mount was cooled in a top-loading dilution refrigerator achieving temperatures down to 0.1 K. The ND data were collected at 0.1, 1.5, and 160 K using an incident neutron beam of wavelength $\lambda = 2.4586$ Å, counting for about 8 h at each temperature.

The μSR measurements were performed at the ISIS facility, Rutherford Appleton Laboratory, Didcot, UK using the spectrometer MuSR. The powdered $Tb_2Hf_2O_7$ sample was mounted on a high-purity silver plate using diluted GE varnish which was then covered with a thin silver foil. A dilution refrigerator was used to cool the sample down to 0.3 K. The μSR data were collected at several temperatures between 0.3 and 20 K in zero field, and at 0.3, 1, 2, and 4 K in longitudinally applied fields up to 0.3 T.

III. CRYSTALLOGRAPHY

The room-temperature powder XRD pattern of $Tb_2Hf_2O_7$ is shown in Fig. 1 along with the Rietveld refinement profile using the $Eu_2Zr_2O_7$-type face-centered-cubic (space group $Fd\bar{3}m$) pyrochlore structure. The refinement reflects the single-phase nature of the sample without any detectable impurity. The lattice parameter is found to be $a = 10.4635(1)$ Å and the relative x coordinate of O1 is $x_{O1} = 0.353(2)$. The atomic position of Tb, Hf, O1, and O2 associated with the Wyckoff positions
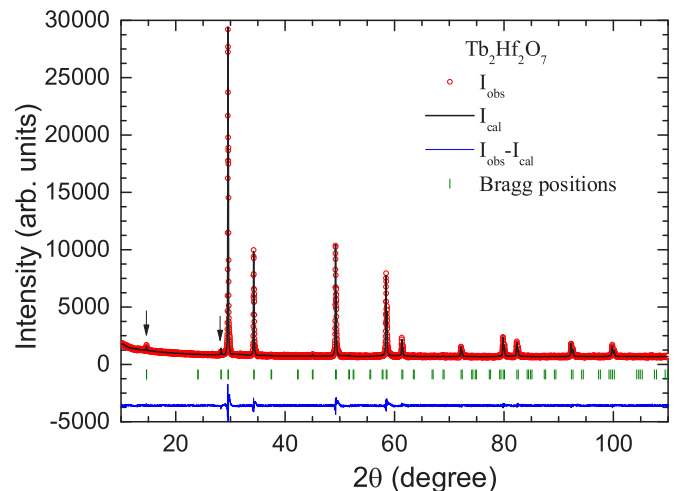

FIG. 1. X-ray powder diffraction pattern of polycrystalline $Tb_2Hf_2O_7$ recorded at room temperature. The solid line through the experimental points is the Rietveld refinement profile calculated for the $Eu_2Zr_2O_7$-type face-centered-cubic (space group $Fd\bar{3}m$) pyrochlore structure. The short vertical bars mark the Bragg-peak positions and the lowermost curve represents the difference between the experimental and calculated intensities. The arrows mark pyrochlore superlattice reflections.

are $16d$ (1/2,1/2,1/2), $16c$ (0,0,0), $48f$ (x_{O1},1/8,1/8), and $8b$ (3/8,3/8,3/8), respectively. The values of a and x_{O1} obtained from the refinement agree very well with those reported in literature [31].

Even though we refined the XRD data within the pyrochlore structure, we would like to point out that $Tb_2Hf_2O_7$ does not have a well-ordered pyrochlore structure. Considering the ratio of the cation radii $r_{Tb}/r_{Hf} \approx 1.46$ which is at the boundary of the values (1.46–1.78) suggested for a stable ordered pyrochlore phase [35], the pyrochlore structure might not be stable and a defect fluorite phase may form as the smaller values of ratio of the cation radii have been found to favor the defect fluorite structure formation. This structural instability was noticed by Karthik *et al.* [31] through high-resolution transmission electron microscopy imaging studies. In their structural studies of $R_2Hf_2O_7$, they noticed a systematic transformation from the well-ordered pyrochlore ($Fd\bar{3}m$ space group) phase to fluorite ($Fm\bar{3}m$ space group) phase as the series progresses from La to Lu. In the defect fluorite structure, the local O surroundings for both cations (R^{3+} and Hf^{4+}, occupying cubic sites) are identical with the eight O atoms located at tetrahedral sites [35]. On the other hand, in a pyrochlore structure, the O surroundings of eightfold coordinated R^{3+} changes to scalenohedra (distorted cubic) consisting of two shorter and six longer R-O distances, whereas the O surroundings for sixfold-cordinated Hf^{4+} changes to trigonal antiprisms (distorted octahedral) [35]. $Tb_2Hf_2O_7$ lies at the boundary of pyrochlore and defect-fluorite structure. Nevertheless, the characteristic pyrochlore peaks, although weak, are clearly seen in the XRD pattern (marked with arrows in Fig. 1).

Very recently, Sibille *et al.* [33] found evidence for Frenkel pair defects/anion disorder using combined resonant x-ray and neutron powder diffraction studies. They report $8 \pm 0.5\%$ oxygen vacancy at the $48f$ site compensated by an oxygen occupancy of $49 \pm 3\%$ at the $8a$ (1/8,1/8,1/8) site (this site is unoccupied in an ideal pyrochlore structure) [33]. In order to get a rough estimate we also tried to refine the occupancy at the $48f$ and $8a$ sites which yielded an O vacancy of $10 \pm 3\%$ at the $48f$ site and an O occupancy of $51 \pm 9\%$ for the $8a$ site. These numbers agree with those of Sibille *et al.* [33] and suggest the presence of a similar level of disorder in both samples.

The order-disorder transition can change the crystal-field environment and introduce a bond disorder, and hence influence the physical properties of a system. The crystal-field anisotropy has a key role in the development of magnetic frustration on a corner-sharing tetrahedra of a pyrochlore. In the case of $Tb_2Ti_2O_7$ it is the low-lying excited crystal-field level which is believed to renormalize the effective Hamiltonian for quantum spin-ice state [20,21]. The inelastic neutron scattering experiments have revealed the splitting energies between the ground-state doublet and the first excited doublet in $Tb_2Ti_2O_7$ and $Tb_2Sn_2O_7$ to be 1.41 and 1.28 meV, respectively [32]. In contrast to discrete CEF excitations in $Tb_2Ti_2O_7$ and $Tb_2Sn_2O_7$, a rather broad CEF excitation is found in inelastic neutron scattering of $Tb_2Hf_2O_7$ for which Sibille *et al.* [33] suggest a splitting energy of at least 4.3 meV. Our heat capacity data (discussed latter) suggests a first excited state near 11 meV. This reflects a strong modification in CEF states brought by the presence of disorder in the pyrochlore structure of $Tb_2Hf_2O_7$.

IV. ac MAGNETIC SUSCEPTIBILITY

The ac magnetic susceptibility $\chi_{ac}(T)$ data of $Tb_2Hf_2O_7$ are shown in Fig. 2. Both real χ' and imaginary χ'' parts of $\chi_{ac}(T)$
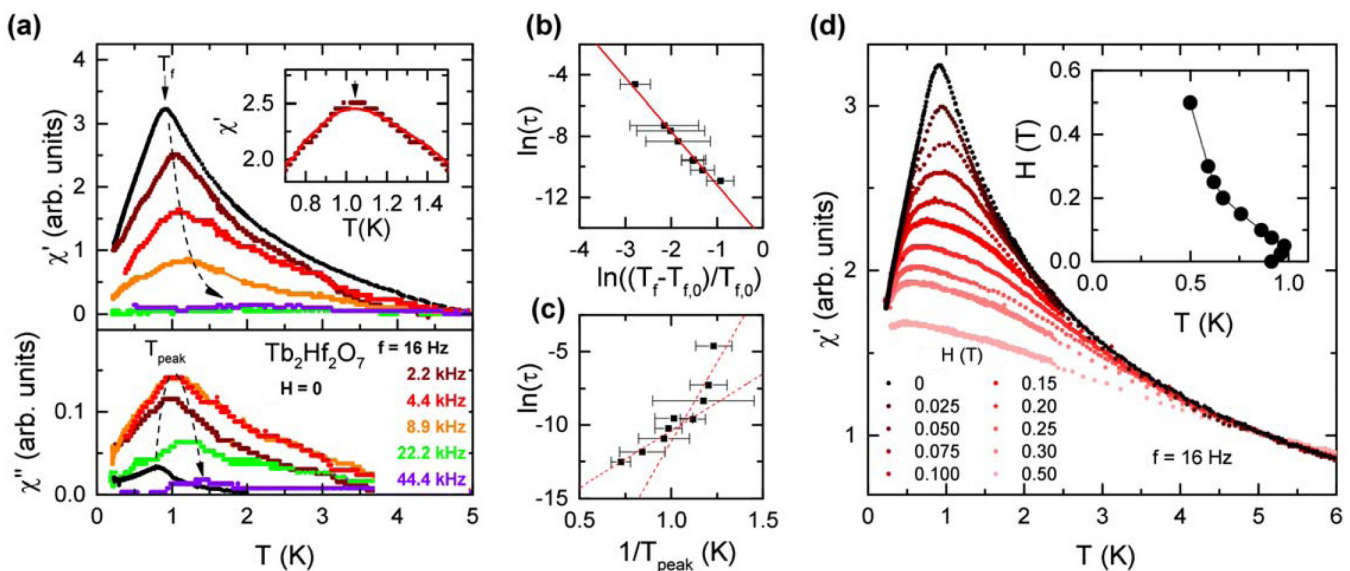

FIG. 2. (a) Real χ' and imaginary χ'' parts of the ac magnetic susceptibility of polycrystalline $Tb_2Hf_2O_7$ as a function of temperature T between 0.1 and 5 K measured at the indicated frequencies f and zero dc magnetic field. Inset: ac susceptibility measured at 2.2 KHz using adiabatic demagnetization cooling (dots) compared to a measurement at 2.3 kHz using zero-field cooling (solid line). (b) The frequency dependence of the freezing temperature T_f plotted as $\ln(\tau)$ versus $\ln(t)$, where $\tau = 1/(2\pi f)$ and the reduced temperature $t = (T_f - T_{f,0})/T_{f,0}$. The solid line represents the fit mentioned in the text. (c) Logarithmic spin-relaxation time τ versus inverse peak temperature. Dashed lines indicate Arrhenius fits. (d) $\chi'(T)$ for different applied dc fields H at 16 Hz under a field-cooled condition. Inset: H-T phase diagram for $T_f(H)$.

show frequency-dependent broad peaks. The peak position does not depend on the cooling protocol [inset of Fig. 2(a)]. At similar frequencies the maximum in χ' and χ'' coincide for cooling through adiabatic demagnetization as well as cooling under zero magnetic field using a dilution refrigerator equipped with a compensated coil-pair susceptometer. At 16 Hz, the peak in χ' is centered at $T_f = 0.91$ K accompanied by a peak at $T_{peak} = 0.81$ K in χ'' [Fig. 2(a)]. With increasing frequency the peak positions of both χ' and χ'' shift to higher temperatures. Such frequency-dependent shift is a well-known feature of spin-glass and spin-ice systems [1,36].

The relative shift in freezing temperature per decade of frequency $\delta T_f = \Delta T_f/[T_f \Delta(\log f)] = 0.06(1)$ for $Tb_2Hf_2O_7$ is comparable to that of insulating spin glasses such as $Eu_xSr_{1-x}S$ and $CoO \cdot Al_2O_3 \cdot SiO_2$ [36] and the metallic ferromagnetic cluster spin-glass $PrRhSn_3$ [37]. A similar value of δT_f (0.06–0.08) was found for $Tb_2Ti_2O_7$ [38]. $T_f(f)$ follows a conventional power-law divergence of critical slowing down, $\tau = \tau_0 t^{-z\nu}$ [where $\tau = 1/(2\pi f)$ and $t = (T_f - T_{f,0})/T_{f,0}$ with $T_{f,0} \approx 0.86$ K; ν being the critical exponent of the correlation length $\xi = (T_f/T_{f,0} - 1)^{-\nu}$ and $\tau \sim \xi^z$] with a critical exponent $z\nu = 3.5(2)$. A plot of $\ln(\tau)$ versus t is shown in Fig. 2(b) along with the fit for parameters $z\nu = 3.5$ and $\tau_0 = 4 \times 10^{-7}$ s. Thus the ac susceptibility suggest a spin-glass-type freezing in $Tb_2Hf_2O_7$.

In order to understand the spin relaxation in $Tb_2Hf_2O_7$, we analyze the frequency dependence of T_{peak} in the dissipative part χ''. The $\tau(T)$ is shown in Fig. 2(c), plotted as $\ln(\tau)$ versus $1/T_{peak}$. We find that the frequency dependence of T_{peak} does not follow a simple Arrhenius law, $\tau = \tau_0 \exp(E_b/k_B T)$, where E_b is the thermal energy barrier [see Fig. 2(c)]. An analysis of the Pearson correlation coefficient showed that a single Arrhenius fit leads to only 0.907 while the dynamical scaling law leads to an excellent correlation of -0.991. Sibille *et al.* [33] also report a non-Arrhenius behavior for the spin freezing in $Tb_2Hf_2O_7$. This kind of non-Arrhenius behavior has also been observed in the spin-ice system $Dy_2Ti_2O_7$ [39] and spin-liquid system $Tb_2Ti_2O_7$ [38] suggesting that the spin relaxation is not simply thermally activated by one energy barrier.

We performed partial linear fits of $\ln(\tau)$ versus $1/T_{peak}$ in two different T regions [as shown in Fig. 2(c)] which yield the energy barriers 7.8 and 22 K. For the spin-ice system $Ho_2Ti_2O_7$, an energy barrier of 27.5 K has been found by analyzing the f dependence of T_f by Arrhenius law [40]. For $Dy_2Ti_2O_7$ an energy barrier of 6.6 K was found to fit the spin relaxation in the low-T regime [41]. In the case of $Tb_2Ti_2O_7$, the f dependence of T_f was analyzed by $\tau = \tau_0 \exp[(E_b/k_B T)^\sigma]$ which yielded $E_b \approx 0.91$ K with $\sigma \approx 2$ [38].

In order to gain more insight into the spin dynamics of $Tb_2Hf_2O_7$ we also measured the ac susceptibility under applied dc magnetic fields, which is shown in Fig. 2(d). At $H \leqslant 0.05$ T, T_f shifts to slightly higher temperatures. However, at fields higher than 0.05 T, T_f shifts to lower temperatures. The field dependence of T_f is summarized in the H-T phase diagram in the inset of Fig. 2(d). While the suppression of T_f by fields is similar to the cooperative freezing behavior in spin glasses, the increase of T_f at low H cannot be understood by spin-glass physics. An increase of T_f with field has been observed in the spin-ice systems $Dy_2Ti_2O_7$ [39] and $Ho_2Ti_2O_7$ [42].

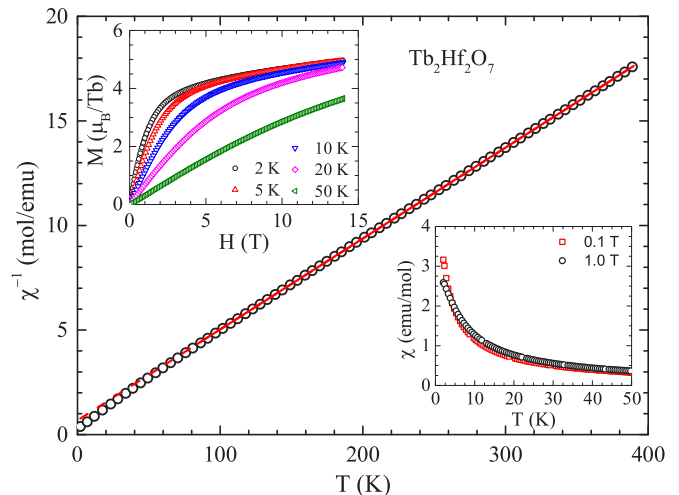

FIG. 3. Zero-field-cooled magnetic susceptibility χ of polycrystalline $Tb_2Hf_2O_7$ plotted as inverse magnetic susceptibility χ^{-1} as a function of temperature T for $2\,K \leqslant T \leqslant 390\,K$ measured in magnetic field $H = 1.0$ T. The solid red line is a Curie-Weiss fit for $50\,K \leqslant T \leqslant 390\,K$ and the dashed line is the extrapolation of the fit toward 0 K. Lower inset: Low-T $\chi(T)$ data measured in $H = 0.1$ and 1.0 T. Upper inset: Isothermal magnetization $M(H)$ for $0 \leqslant H \leqslant 14$ T measured at the indicated temperatures.

The complex field dependence of T_f reflects a complex spin dynamics in $Tb_2Hf_2O_7$.

V. dc MAGNETIC SUSCEPTIBILITY AND MAGNETIZATION

The zero-field-cooled (ZFC) dc magnetic susceptibility $\chi(T)$ of $Tb_2Hf_2O_7$ is shown in Fig. 3 for $2\,K \leqslant T \leqslant 390\,K$. Consistent with $\chi_{ac}(T)$, no anomaly related to a magnetic phase transition is seen in $\chi(T)$ data, although the magnitude of χ at low T is rather large (see the lower inset of Fig. 3) as commonly seen in the $R_2B_2O_7$ pyrochlores. No thermal hysteresis was observed between the ZFC and field-cooled $\chi(T)$ data (not shown) above 2 K. The $\chi(T)$ data follow a Curie-Weiss behavior, $\chi(T) = C/(T - \theta_p)$. A fit of the ZFC $\chi^{-1}(T)$ data between 50 and 390 K, measured in 1.0 T, shown by the solid red line in Fig. 3, yields $C = 11.47(3)$ emu K/mol Tb and $\theta_p = -14.6(5)$ K. The effective moment obtained from C, $\mu_{eff} \approx 9.58(2)\mu_B/Tb$, is very close to the expected value of $9.72\mu_B$ for free Tb^{3+} ions. The negative value of θ_p indicates an antiferromagnetic interaction in $Tb_2Hf_2O_7$. The $\chi^{-1}(T)$ data when fitted in the T range of 15–30 K yields $C = 10.03(2)$ emu K/mol Tb and $\theta_p = -6.10(4)$ K, thus an effective moment of $8.96\mu_B$ is obtained for the low-temperature ground state.

The isothermal magnetization $M(H)$ collected at five selected temperatures between 2 and 50 K is shown in the upper inset of Fig. 3. At low temperatures, M increases rapidly at low H and weakly at higher H. At 2 K and 14 T the magnetization attains a value of $M \approx 4.9\mu_B/Tb$ which is only about 54% of the theoretical saturation magnetization of $9\mu_B/Tb$ for free Tb^{3+} ions. Such a low value of M suggests the presence of strong single-ion anisotropy. Further, it is seen that the $M(H)$ shows slight nonlinearity even at 50 K which can be attributed to the combined effect of crystal field and saturation tendency.
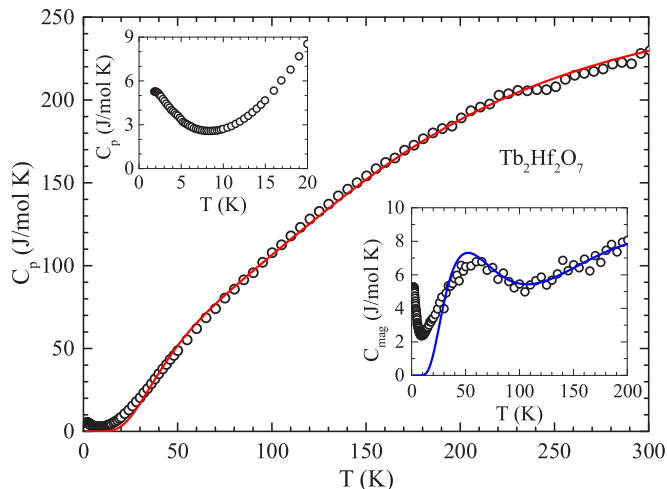
FIG. 4. Heat capacity C_p of polycrystalline $Tb_2Hf_2O_7$ as a function of temperature T between 1.8 and 300 K, measured in zero field. The solid red curve is the fit by Debye + Einstein models of lattice heat capacity plus crystal-field contribution. Upper inset: Expanded view of low-T $C_p(T)$ data between 1.8 and 20 K. Lower inset: Magnetic contribution to heat capacity $C_{mag}(T)$ of $Tb_2Hf_2O_7$. The solid blue curve represents the crystal-field contribution to heat capacity.

We also notice that even at 2 K the M does not fully saturate up to 14 T; instead it shows a weak increase with increasing H. This could be the effect of CEF and/or the presence of disorder.

We would like to point out that the $M(H)$ data could not be described by the effective spin-half model of local $\langle 111 \rangle$ Ising anisotropy observed in Ising pyrochlores such as in $Dy_2Ti_2O_7$ [43], $Nd_2Zr_2O_7$ [14], and $Nd_2Hf_2O_7$ [15]. It appears that the presence of anion disorder modifies the crystal-field anisotropy leading to the departure from the expected Ising-type anisotropy in $Tb_2Hf_2O_7$.

VI. HEAT CAPACITY

The heat capacity $C_p(T)$ of $Tb_2Hf_2O_7$ is shown in Fig. 4 for 1.8 K $\leqslant T \leqslant$ 300 K. The $C_p(T)$ data show no anomaly related to a phase transition down to 1.8 K. However, as visualized in the upper inset, the $C_p(T)$ data show an upturn below about 8 K that might indicate the precursor of magnetic order. Further, it is seen that the $C_p(T)$ tends to flatten below 2 K, possibly indicating the occurrence of a peak below 2 K.

The magnetic contribution to the heat capacity $C_{mag}(T)$, which was estimated by subtracting off the lattice contribution, is shown in the lower inset of Fig. 4. For the lattice contribution we used the heat capacity of nonmagnetic $La_2Hf_2O_7$ [15] after correcting for the small difference in formula masses and unit cell volumes of $La_2Hf_2O_7$ and $Tb_2Hf_2O_7$. The $C_{mag}(T)$ exhibits a broad Schottky-type peak near 55 K. The $C_{mag}(T)$ data below 200 K is reasonably described by a three-level CEF scheme. The analysis of $C_{mag}(T)$ data suggests the ground state to be a doublet with a first excited doublet at around 125 K and a quasiquartet state at around 710 K. The CEF contribution to heat capacity $C_{CEF}(T)$ is shown by the solid blue curve in the lower inset of Fig. 4. A nice agreement is seen between $C_{mag}(T)$ and $C_{CEF}(T)$ above 20 K where the interactions between Tb^{3+}

ions are insignificant and the Schottky-type feature is well accounted for.

The inelastic neutron scattering data of $Tb_2Hf_2O_7$ do not show discrete CEF excitations; instead, broad inelastic signals (mostly between 5 and 25 meV) are observed [33], which can be attributed to a distribution of crystal-field environments around Tb^{3+}. Sibille *et al.* [33] suggested an energy gap of at least 4.3 meV (50 K) for the first excited state. The raw inelastic neutron scattering data show a rather broad CEF excitation between 5 and 10 meV (associated with the first excited state), which is somewhat smaller than our estimate of 11 meV (125 K) from the heat capacity.

The high-temperature $C_p(T)$ data show that the C_p does not reach the Dulong-Petit value of $C_V = 3nR = 33R \approx$ 274.4 J/mol K by 300 K ($C_p \sim$ 225 J/mol K). This is consistent with the large value of Debye temperature Θ_D observed in the $R_2B_2O_7$ pyrochlore family. A fit of the $C_p(T)$ data by a combination of the Debye and Einstein models of lattice heat capacity added to the fixed crystal-field contribution $C_{CEF}(T)$ (according to the CEF level scheme discussed above) [44] shown by the solid red curve in Fig. 4 gives Θ_D = 787(6) K and Einstein temperature Θ_E = 163(3) K with 66% weight to Debye term and 34% to Einstein term. The value of Θ_D obtained compares with that of the other pyrohafnates $La_2Hf_2O_7$ [Θ_D = 792(5) K] [15], $Nd_2Hf_2O_7$ [Θ_D = 785(6) K] [15] and $Pr_2Hf_2O_7$ [Θ_D = 790(7) K] [29].

VII. NEUTRON POWDER DIFFRACTION: DIFFUSE SCATTERING

Neutron powder diffraction patterns of $Tb_2Hf_2O_7$ collected at 0.1 and 1.5 K are shown in Fig. 5(a). No magnetic Bragg peaks are observed in ND data down to 0.1 K; however, a broad shoulderlike feature is seen at lower Q which is more clearly seen in the expanded plot shown in Fig. 5(b). This broad shoulder arises due to magnetic diffuse scattering as a result of the development of short-range magnetic correlations at low temperatures. A similar feature in ND data has also been observed for the spin-liquid $Tb_2Ti_2O_7$ [16,17]. In order to better resolve the magnetic diffuse scattering we subtracted the ND data taken at 160 K from those taken at 0.1 K. The magnetic intensity at 0.1 K is shown in Fig. 6 (the featureless paramagnetic scattering was added according to [45] after subtraction). The sharp decrease of diffuse scattering intensity when Q is approaching zero indicates dominant antiferromagnetic correlations, consistent with the negative Weiss temperature.

The broad peak near $Q \sim$ 1.2 Å^{-1} (Fig. 6) corresponds to the nearest-neighbor spin correlations with a distance 3.7 Å. The large peak width indicates that the spin correlations exist only over a very short range. The powder-averaged scattering due to the nearest-neighbor isotropic spin correlations could be described by [46]

$$I(Q) \sim f(Q)^2 \frac{\sin(Qr_{ij})}{Qr_{ij}}, \qquad (1)$$

where $f(Q)^2$ is the magnetic form factor of Tb^{3+} and $r_{ij} \approx$ 3.7 Å is the nearest-neighbor distance. As shown in Fig. 6, the model qualitatively accounts for the modulation of the
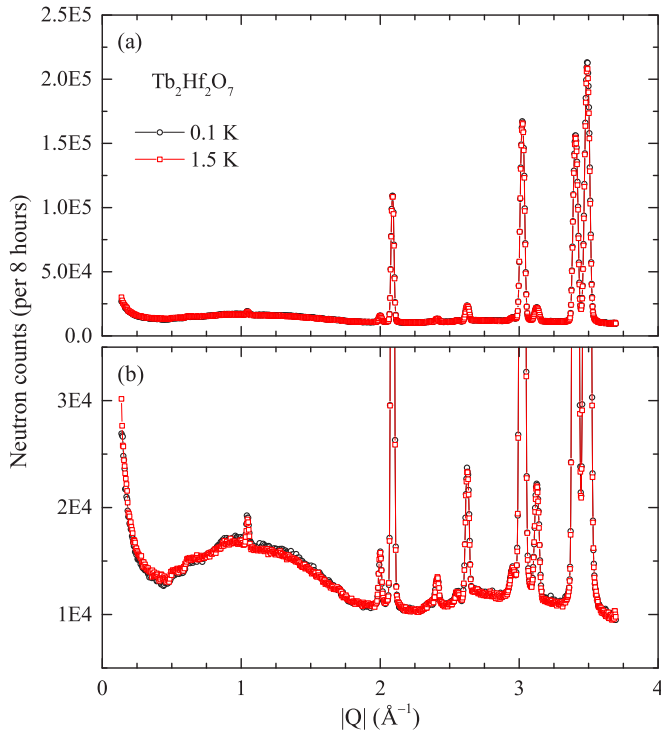
FIG. 5. (a) Neutron powder diffraction patterns of $Tb_2Hf_2O_7$ collected at 0.1 and 1.5 K. (b) Expanded *y*-scale plot showing the broad shoulderlike feature at low $|Q|$ due to magnetic diffuse scattering.

FIG. 6. Magnetic diffuse neutron scattering pattern of $Tb_2Hf_2O_7$ at 100 mK obtained by subtracting the 160 K data from the data at 100 mK, calculated powder-averaged scattering pattern due to nearest-neighbor isotropic antiferromanetic spin correlations (green line), and reverse Monte Carlo (RMC) fit (red line) and the difference (blue line). Inset: The reconstructed diffraction pattern in the (*hhl*) reciprocal plane based on the fitted spin configurations.

intensity which suggests that the spin correlations only extend over nearest neighbors.

In order to gain further insight on the short-range spin correlations and spin anisotropy in $Tb_2Hf_2O_7$, the magnetic diffuse scattering pattern was analyzed with the reverse Monte Carlo (RMC) method. The RMC algorithm describes the experimental powder magnetic diffuse scattering data by a large configuration of classical spin vectors with certain anisotropy. During the refinement, the orientations of the spins are refined in order to describe best the experimental data. The program SPINVERT [47] is used which has been successfully applied to several frustrated magnetic systems and reveals many before-unnoticed novel types of spin correlations [47–50]. In our calculations, a $6 \times 6 \times 6$ supercell is generated (in total 3456 spins) with randomly oriented magnetic moments (isotropic spins) assigned to each magnetic Tb^{3+} site. In total 500 moves per spin are considered for a refinement and ten individual fits have been performed to ensure the robustness of the results.

The fitted magnetic diffuse scattering pattern with isotropic spins is shown in Fig. 6, which agrees well with the experimental data. The resulting spin configurations were used to reconstruct the Q dependence of the diffuse scattering in the (*hhl*) reciprocal plane (inset of Fig. 6) by using the SPINDIFF program which is an extension to the SPINVERT program. The calculated pattern is quite similar to the experimentally observed pattern obtained from the single crystal diffuse neutron scattering of $Tb_2Hf_2O_7$ reported by Sibille *et al.* [33]. The fitted spin configurations reveal that the spins are generally antiferromagnetically correlated, which is consistent with the negative Weiss temperature.
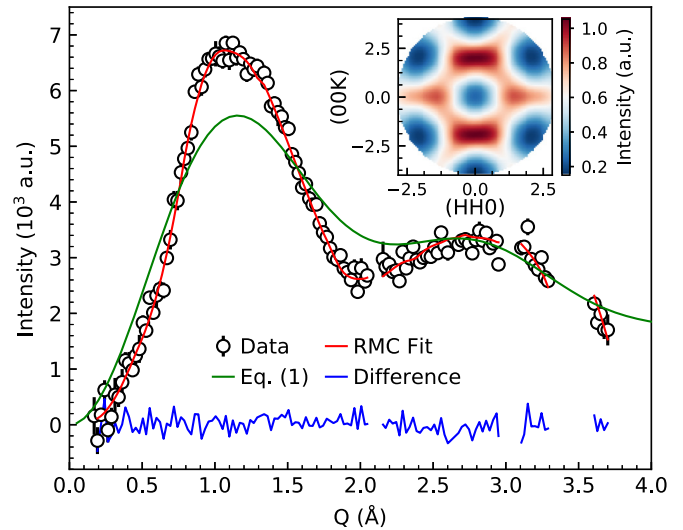
We would like to mention that we also performed refinements with spins of local $\langle 111 \rangle$ Ising anisotropy as well as easy-plane anisotropy. The Ising anisotropy case did not yield an acceptable fit. Considering easy-plane anisotropy is also found to give a fit quality similar to the one with isotropic spins; however, the calculated single crystal scattering pattern based on the refined spin configurations differs significantly from the observed pattern in Ref. [33]. This leaves the refinement with isotropic spins as the only acceptable solution which reflects the non-Ising character of anisotropy of Tb^{3+} in $Tb_2Hf_2O_7$, possibly because of the mixing of the CEF ground state with excited states by exchange interactions and the structural disorder.

VIII. MUON SPIN RELAXATION

In order to obtain further insight into the spin dynamics of $Tb_2Hf_2O_7$, we also carried out μSR measurements. The μSR data were reduced and analyzed using the program MANTID [51]. The μSR spectra of $Tb_2Hf_2O_7$ collected in zero field (ZF) are shown in Fig. 7 for a few representative temperatures between 0.3 and 20 K. The μSR spectra do not show any signature of long-range magnetic order (no oscillations related to muon spin precession) or a static ground state (no $2/3$ loss in asymmetry compared to its high-T value). Thus, consistent with the above neutron data, the muons also do not see a magnetic ordering down to 0.3 K. The μSR spectra are well described by a stretched exponential relaxation function, $G_z(t) = A_0 \exp[(-\lambda t)^\beta] + A_{BG}$, where A_0 is the initial asymmetry, λ is the depolarization rate, and β is the exponent. In the fast fluctuations limit, λ is related to the spin-
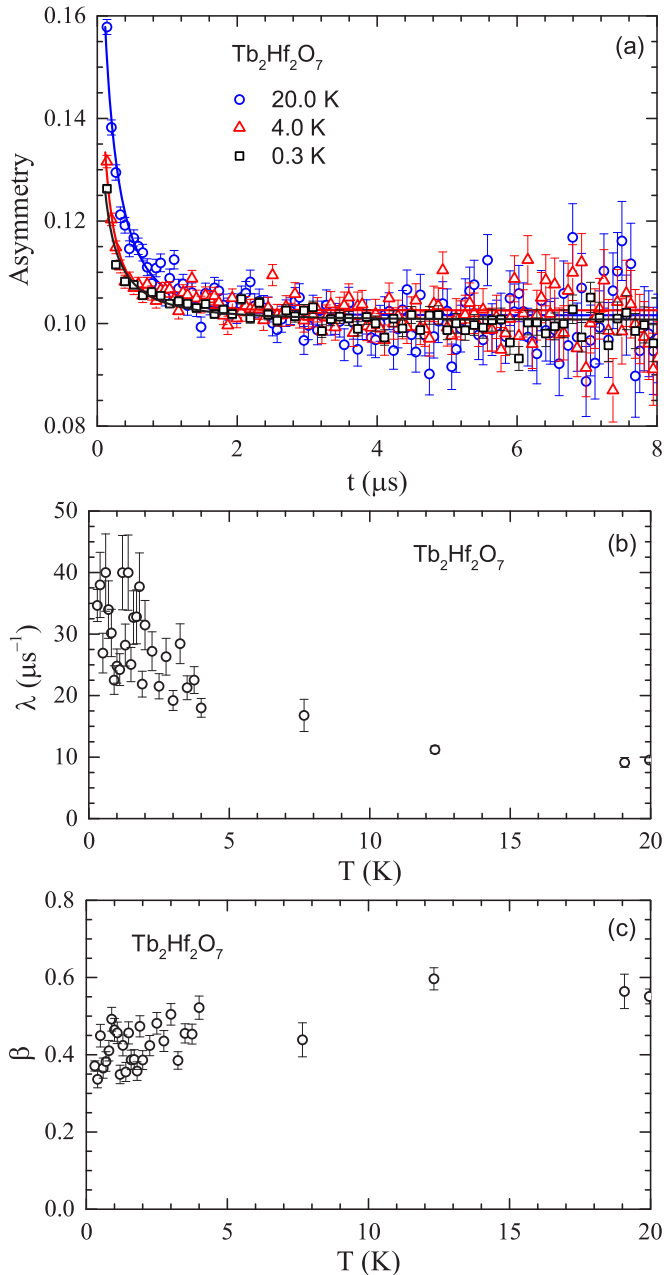
FIG. 7. (a) Zero-field (ZF) muon spin asymmetry function G_z versus time t spectra of $Tb_2Hf_2O_7$ at few representative temperatures. Solid curves are the fits to the μSR data by a stretched exponential relaxation function, $G_z(t) = A_0 \exp[(-\lambda t)^\beta] + A_{BG}$. (b) Temperature T dependence of depolarization rate λ, and (c) T dependence of exponent β, obtained from the analysis of the ZF μSR data at $0.3 \leqslant T \leqslant 20$ K.

fluctuation rate ν which in Redfield formalism is given by [52]

$$\lambda = \frac{2\gamma_\mu^2 H_\mu^2 \nu}{\nu^2 + \gamma_\mu^2 H_{LF}^2}, \qquad (2)$$

where γ_μ is the muon gyromagnetic ratio, H_μ is the magnitude of the fluctuating field at the muons site, and H_{LF} is the applied longitudinal field. For a dynamic relaxation one expects $\beta = 1$ (exponential relaxation function), whereas for the static or

quasistatic case one would expect $\beta = 2$. When there is a distribution of dynamic relaxation channels, β is less than 1.

The fits of the representative μSR spectra are shown by the solid curves of respective colors in Fig. 7(a). The parameters λ and β obtained from the fits are shown in Figs. 7(b) and 7(c), respectively. It is seen that λ tends to increase with decreasing temperature. According to Eq. (2), for zero field $\lambda \sim 1/\nu$, therefore an increase in λ implies a decrease in the spin-fluctuation rate and, hence, a slowing down of spin dynamics. The value of β is much lower than 1 and suggests a distribution of relaxation channels. Thus, from the ZF μSR data we conclude the existence of slow spin dynamics and persistent spin fluctuations. Our findings are similar to those of Sibille *et al.* [33] who also reported a slowing down of spin dynamics and coexisting spin fluctuations in the macroscopically frozen state of $Tb_2Hf_2O_7$ through their ZF μSR study.

Figure 8(a) shows the longitudinal-field (LF) μSR asymmetry spectra of $Tb_2Hf_2O_7$ for a few representative fields between 5 and 300 mT collected at 0.3 K. For comparison, the ZF μSR data at 0.3 K are also shown. From the raw spectra [Fig. 8(a)] we see that there is almost no change in the initial asymmetry for fields up to 300 mT. The LF μSR spectra are also well described by the stretched exponential relaxation function. The fits are shown by the solid curves in Fig. 8(a). The fit parameters for the LF data collected at 0.3, 1.0, 2.0, and 4.0 are shown in Figs. 8(b) and 8(c). A comparison of the fit parameters for ZF spectra in Fig. 7 and LF spectra in Fig. 8 shows that with the application of field the values of both λ and β change. While λ decreases, β increases which is noticed even at 5.0 mT field. Further, it is seen that both λ and β show very weak H dependence (almost H independent within the error bar) over 5–300 mT. Thus, the H-dependent behavior of the muon relaxation does not follow Eq. (2) according to which one would expect a decrease in λ with increasing H_{LF}. This suggests that the spin dynamics in $Tb_2Hf_2O_7$ is more complicated than that described by Eq. (2). We further notice that fields up to 300 mT are not sufficient to restore the initial polarization. This suggests a dynamic nature of the muon relaxation in $Tb_2Hf_2O_7$. Much higher fields have been suggested to restore the initial polarization when the muon relaxation is dynamic in nature [53].

IX. CONCLUSIONS

We have investigated the physical properties of $Tb_2Hf_2O_7$ using $\chi_{ac}(T)$, $\chi(T)$, $M(H)$, $C_p(T)$, μSR, and neutron powder diffraction measurements. The $\chi(T)$ and $C_p(T)$ show no anomaly related to a magnetic phase transition down to 1.8 K. The negative θ_p obtained from the analysis of $\chi(T)$ indicates a dominant antiferromagnetic interaction. The $M(H)$ data reflect strong single-ion anisotropy. The $C_p(T)$ shows an upturn below 8 K. Clear evidence for a slowing down of spin dynamics is provided by $\chi_{ac}(T)$ data. The frequency- and field-dependent $\chi_{ac}(T)$ data reveal complex spin dynamics in $Tb_2Hf_2O_7$. The μSR data follow a stretched exponential behavior reflecting a slow spin dynamics and persistent spin fluctuations down to 0.3 K with a distribution of relaxation channels. The $\chi_{ac}(T)$ and μSR data together provide evidence for coexisting persistent dynamic spin fluctuations inside the macroscopically spin-frozen state. The powder neutron diffraction shows magnetic diffuse scattering which has been analyzed by the RMC method
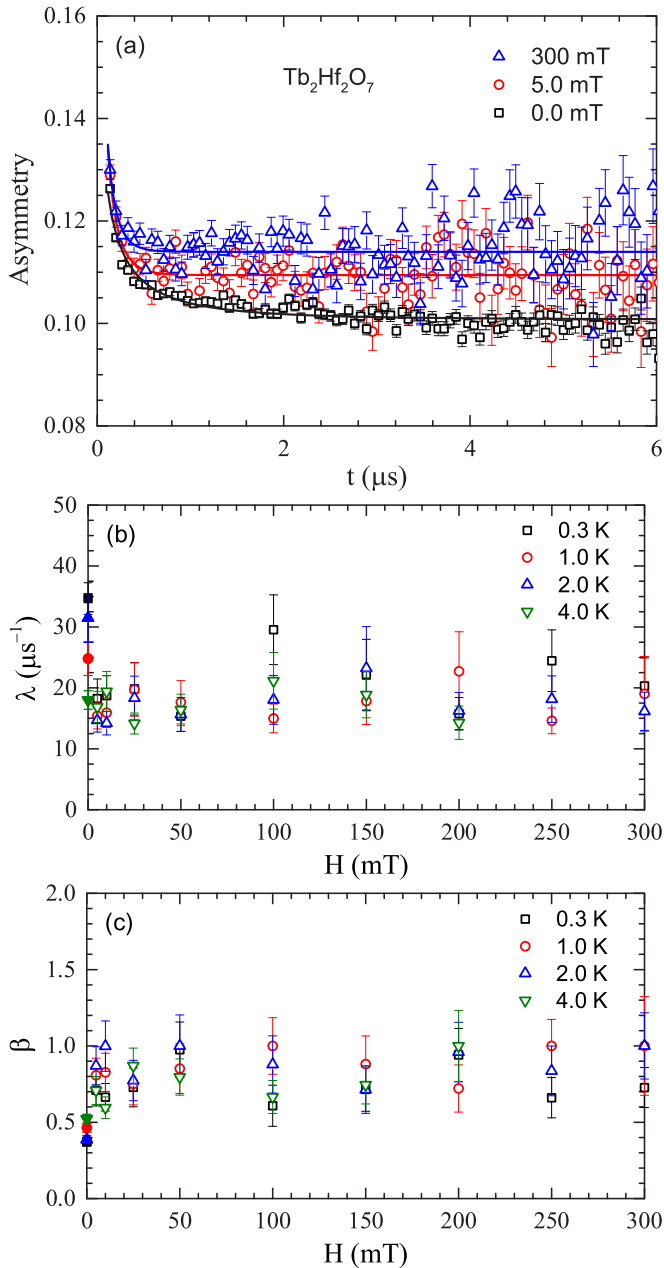
FIG. 8. (a) Longitudinal-field (LF) muon spin asymmetry function G_z versus time t spectra of $Tb_2Hf_2O_7$ at 0.3 K for a few representative fields. Solid curves are the fits to the μSR data by a stretched exponential relaxation function, $G_z(t) = A_0 \exp[(-\lambda t)^\beta] + A_{BG}$. (b) Magnetic field H dependence of the depolarization rate λ, and (c) H dependence of the exponent β, obtained from the analysis of the LF μSR data. The data points at $H = 0$ (solid symbols) in (b) and (c) correspond to the parameters λ and β for zero-field μSR data in Fig. 7.

and a dominant antiferromagnetic correlation is inferred. The RMC analysis also shows approximately isotropic spins rather than Ising anisotropy. Altogether our investigations reveal a dynamical ground state in $Tb_2Hf_2O_7$.

The evidence for the existence of a dynamical ground state found by us, is consistent with the recently proposed Coulomb spin-liquid behavior by Sibille *et al.* [33]. Sibille *et al.* [33] as well observe a frequency-dependent $\chi_{ac}(T)$ and a non-Arrhenius behavior for spin freezing in $Tb_2Hf_2O_7$. They suggested a spin-glass-type freezing, which, however, is not supported by our $\chi_{ac}(T)$ data collected with applied dc magnetic field. Sibille *et al.* [33] also find evidence for a dynamic nature of magnetism in $Tb_2Hf_2O_7$ in their μSR study. They suggested a macroscopically frozen state to coexist with fast fluctuations which we as well infer from our μSR results. Sibille *et al.* [33] further observe magnetic diffuse scattering as a result of the development of short-range spin-spin correlations. This is again consistent with our observation of diffuse scattering. In addition, Sibille *et al.* [33] probe spin correlations using low-energy inelastic neutron scattering which provides evidence for a Coulomb phase, characterized by power-law correlations.

Our investigations suggest the ground-state properties of $Tb_2Hf_2O_7$ to have some similarities with those of the spin-liquid candidate $Tb_2Ti_2O_7$, although the pyrochlore structure of $Tb_2Hf_2O_7$ is found to have disorder. They both have dominating antiferromagnetic interaction, show non-Arrhenius behavior in ac susceptibility measurement, diffuse magnetic scattering in neutron diffraction measurement, and stretched exponential behavior in muon spin relaxation measurement. On the other hand, magnetic heat capacity as well as inelastic neutron scattering data of $Tb_2Hf_2O_7$ [33] suggest a first excited state much higher than that in $Tb_2Ti_2O_7$ for which the first excited CEF level at around 1.4 meV has been proposed to renormalize the effective low-energy spin Hamiltonian leading to a quantum spin-ice state in $Tb_2Ti_2O_7$ [20,21]. It appears that the presence of disorder plays an important role in the dynamical behavior of $Tb_2Hf_2O_7$. As such, $Tb_2Hf_2O_7$ seems to be a potential compound for further investigations to understand the role of disorder on the spin dynamics in these pyrochlores.

[1] J. S. Gardner, M. J. P. Gingras, and J. E. Greedan, Magnetic pyrochlore oxides, Rev. Mod. Phys. **82**, 53 (2010).

[2] M. J. P. Gingras and P. A. McClarty, Quantum spin ice: A search for gapless quantum spin liquids in pyrochlore magnets, Rep. Prog. Phys. **77**, 056501 (2014).

[3] C. Castelnovo, R. Moessner, and S. L. Sondhi, Spin ice, fractionalization, and topological order, Annu. Rev. Condens. Matter Phys. **3**, 35 (2012).

[4] M. J. Harris, S. T. Bramwell, D. F. McMorrow, T. Zeiske, and K. W. Godfrey, Geometrical Frustration in the

Ferromagnetic Pyrochlore $Ho_2Ti_2O_7$, Phys. Rev. Lett. **79**, 2554 (1997).

[5] A. P. Ramirez, A. Hayashi, R. J. Cava, R. B. Siddharthan, and S. Shastry, Zero-point entropy in 'spin ice', Nature (London) **399**, 333 (1999).

[6] R. Siddharthan, B. S. Shastry, A. P. Ramirez, A. Hayashi, R. J. Cava, and S. Rosenkranz, Ising Pyrochlore Magnets: Low-Temperature Properties, Ice Rules, and Beyond, Phys. Rev. Lett. **83**, 1854 (1999).

[7] S. T. Bramwell and M. J. P. Gingras, Spin ice state in frustrated magnetic pyrochlore materials, Science **294**, 1495 (2001).

[8] B. C. Den Hertog and M. J. P. Gingras, Dipolar Interactions and Origin of Spin Ice in Ising Pyrochlore Magnets, Phys. Rev. Lett. **84**, 3430 (2000).

[9] C. Castelnovo, R. Moessner, and S. L. Sondhi, Magnetic monopoles in spin ice, Nature (London) **451**, 42 (2008).

[10] D. J. P. Morris, D. A. Tennant, S. A. Grigera, B. Klemke, C. Castelnovo, R. Moessner, C. Czternasty, M. Meissner, K. C. Rule, J. Hoffmann, K. Kiefer, S. Gerischer, D. Slobinsky, and R. S. Perry, Dirac strings and magnetic monopoles in the spin ice $Dy_2Ti_2O_7$, Science **326**, 411 (2009).

[11] R. G. Melko and M. J. P. Gingras, Monte Carlo studies of the dipolar spin ice model, J. Phys.: Condens. Matter **16**, R1277 (2004).

[12] A. Bertin, P. Dalmas de Réotier, B. Fåk, C. Marin, A. Yaouanc, A. Forget, D. Sheptyakov, B. Frick, C. Ritter, A. Amato, C. Baines, and P. J. C. King, $Nd_2Sn_2O_7$: An all-in/all-out pyrochlore magnet with no divergence-free field and anomalously slow paramagnetic spin dynamics, Phys. Rev. B **92**, 144423 (2015).

[13] E. Lhotel, S. Petit, S. Guitteny, O. Florea, M. Ciomaga Hatnean, C. Colin, E. Ressouche, M. R. Lees, and G. Balakrishnan, Fluctuations and All-In–All-Out Ordering in Dipole-Octupole $Nd_2Zr_2O_7$, Phys. Rev. Lett. **115**, 197202 (2015).

[14] J. Xu, V. K. Anand, A. K. Bera, M. Frontzek, D. L. Abernathy, J. L. Niedziela, N. Casati, K. Siemensmeyer, and B. Lake, Magnetic structure and crystal field states of the pyrochlore antiferromagnet $Nd_2Zr_2O_7$, Phys. Rev. B **92**, 224430 (2015).

[15] V. K. Anand, A. K. Bera, J. Xu, T. Herrmannsdörfer, C. Ritter, and B. Lake, Observation of long-range magnetic ordering in frustrated pyrohafnate $Nd_2Hf_2O_7$: A neutron diffraction study, Phys. Rev. B **92**, 184418 (2015).

[16] J. S. Gardner, S. R. Dunsiger, B. D. Gaulin, M. J. P. Gingras, J. E. Greedan, R. F. Kiefl, M. D. Lumsden, W. A. MacFarlane, N. P. Raju, J. E. Sonier, I. Swainson, and Z. Tun, Cooperative Paramagnetism in the Geometrically Frustrated Pyrochlore Antiferromagnet $Tb_2Ti_2O_7$, Phys. Rev. Lett. **82**, 1012 (1999).

[17] J. S. Gardner, B. D. Gaulin, A. J. Berlinsky, P. Waldron, S. R. Dunsiger, N. P. Raju, and J. E. Greedan, Neutron scattering studies of the cooperative paramagnet pyrochlore $Tb_2Ti_2O_7$, Phys. Rev. B **64**, 224416 (2001).

[18] J. S. Gardner, A. Keren, G. Ehlers, C. Stock, E. Segal, J. M. Roper, B. Fåk, M. B. Stone, P. R. Hammar, D. H. Reich, and B. D. Gaulin, Dynamic frustrated magnetism in $Tb_2Ti_2O_7$ at 50 mK, Phys. Rev. B **68**, 180401(R) (2003).

[19] M. J. P. Gingras, B. C. den Hertog, M. Faucher, J. S. Gardner, S. R. Dunsiger, L. J. Chang, B. D. Gaulin, N. P. Raju, and J. E. Greedan, Thermodynamic and single-ion properties of Tb^{3+} within the collective paramagnetic-spin liquid state of the frustrated pyrochlore antiferromagnet $Tb_2Ti_2O_7$, Phys. Rev. B **62**, 6496 (2000).

[20] H. R. Molavian, M. J. P. Gingras, and B. Canals, Dynamically Induced Frustration as a Route to a Quantum Spin Ice State in $Tb_2Ti_2O_7$ via Virtual Crystal Field Excitations and Quantum Many-Body Effects, Phys. Rev. Lett. **98**, 157204 (2007).

[21] H. R. Molavian, P. A. McClarty, and M. J. P. Gingras, Towards an effective spin hamiltonian of the pyrochlore spin liquid $Tb_2Ti_2O_7$, arXiv:0912.2957.

[22] P. Bonville, I. Mirebeau, A. Gukasov, S. Petit, and J. Robert, Tetragonal distortion yielding a two-singlet spin liquid in pyrochlore $Tb_2Ti_2O_7$, Phys. Rev. B **84**, 184409 (2011).

[23] S. Petit, P. Bonville, J. Robert, C. Decorse, and I. Mirebeau, Spin liquid correlations, anisotropic exchange, and symmetry breaking in $Tb_2Ti_2O_7$, Phys. Rev. B **86**, 174403 (2012).

[24] T. Fennell, M. Kenzelmann, B. Roessli, M. Haas, and R. Cava, Power-Law Spin Correlations in the Pyrochlore Antiferromagnet $Tb_2Ti_2O_7$, Phys. Rev. Lett. **109**, 017201 (2012).

[25] S. Guitteny, J. Robert, P. Bonville, J. Ollivier, C. Decorse, P. Steffens, M. Boehm, H. Mutka, I. Mirebeau, and S. Petit, Anisotropic Propagating Excitations and Quadrupolar Effects in $Tb_2Ti_2O_7$, Phys. Rev. Lett. **111**, 087201 (2013).

[26] K. Fritsch, K. A. Ross, Y. Qiu, J. R. D. Copley, T. Guidi, R. I. Bewley, H. A. Dabkowska, and B. D. Gaulin, Antiferromagnetic spin ice correlations at $(\frac{1}{2}, \frac{1}{2}, \frac{1}{2})$ in the ground state of the pyrochlore magnet $Tb_2Ti_2O_7$, Phys. Rev. B **87**, 094410 (2013).

[27] K. Fritsch, E. Kermarrec, K. A. Ross, Y. Qiu, J. R. D. Copley, D. Pomaranski, J. B. Kycia, H. A. Dabkowska, and B. D. Gaulin, Temperature and magnetic field dependence of spin-ice correlations in the pyrochlore magnet $Tb_2Ti_2O_7$, Phys. Rev. B **90**, 014429 (2014).

[28] V. K. Anand, D. L. Abernathy, D. T. Adroja, A. D. Hillier, P. K. Biswas, and B. Lake, Muon spin relaxation and inelastic neutron scattering investigations of all-in/all-out antiferromagnet $Nd_2Hf_2O_7$, Phys. Rev. B **95**, 224420 (2017).

[29] V. K. Anand, L. Opherden, J. Xu, D. T. Adroja, A. T. M. N. Islam, T. Herrmannsdörfer, J. Hornung, R. Schönemann, M. Uhlarz, H. C. Walker, N. Casati, and B. Lake, Physical properties of a candidate quantum spin-ice system $Pr_2Hf_2O_7$, Phys. Rev. B **94**, 144415 (2016).

[30] R. Sibille, E. Lhotel, M. Ciomaga Hatnean, G. Balakrishnan, B. Fåk, T. Fennell, and M. Kenzelmann, Quantum spin ice in the pyrochlore $Pr_2Hf_2O_7$, Phys. Rev. B **94**, 024436 (2016).

[31] C. Karthik, T. J. Anderson, D. Gout, and R. Ubic, Transmission electron microscopic study of pyrochlore to defect-fluorite transition in rare-earth pyrohafnates, J. Solid State Chem. **194**, 168 (2012).

[32] J. Zhang, K. Fritsch, Z. Hao, B. V. Bagheri, M. J. P. Gingras, G. E. Granroth, P. Jiramongkolchai, R. J. Cava, and B. D. Gaulin, Neutron spectroscopic study of crystal field excitations in $Tb_2Ti_2O_7$ and $Tb_2Sn_2O_7$, Phys. Rev. B **89**, 134410 (2014).

[33] R. Sibille, E. Lhotel, M. Ciomaga Hatnean, G. J. Nilsen, G. Ehlers, A. Cervellino, E. Ressouche, M. Frontzek, O. Zaharko, V. Pomjakushin, U. Stuhr, H. C. Walker, D. T. Adroja, H. Luetkens, C. Baines, A. Amato, G. Balakrishnan, T. Fennell, and M. Kenzelmann, Coulomb spin liquid in anion-disordered pyrochlore $Tb_2Hf_2O_7$, Nat. Commun. **8**, 892 (2017).

[34] J. Rodríguez-Carvajal, Recent advances in magnetic structure determination by neutron powder diffraction, Physica B **192**, 55 (1993); Program Fullprof, LLB-JRC, Laboratoire Léon Brillouin, CEA-Saclay, France, 1996, http://www.ill.eu/sites/fullprof/.

[35] M. A. Subramanian, G. Aravamudan, and G. V. Subba Rao, Oxide pyrochlores: A review, Prog. Solid State Chem. **15**, 55 (1983).

[36] J. A. Mydosh, *Spin Glasses: An Experimental Introduction* (Taylor and Francis, London, 1993).

[37] V. K. Anand, D. T. Adroja, and A. D. Hillier: Ferromagnetic cluster spin-glass behavior in $PrRhSn_3$, Phys. Rev. B **85**, 014418 (2012).

[38] E. Lhotel, C. Paulsen, P. D. de Réotier, A. Yaouanc, C. Marin, and S. Vanishri, Low-temperature magnetization in geometrically frustrated $Tb_2Ti_2O_7$, Phys. Rev. B **86**, 020410(R) (2012).

[39] J. Snyder, B. G. Ueland, J. S. Slusky, H. Karunadasa, R. J. Cava, and P. Schiffer, Low-temperature spin freezing in the $Dy_2Ti_2O_7$ spin ice, Phys. Rev. B **69**, 064414 (2004).

[40] K. Matsuhira, Y. Hinatsu, K. Tenya, and T. Sakakibara, Low temperature magnetic properties of frustrated pyrochlore ferromagnets $Ho_2Sn_2O_7$ and $Ho_2Ti_2O_7$, J. Phys.: Condens. Matter **12**, L649 (2000).

[41] L. D. C. Jaubert and P. C. W. Holdsworth, Magnetic monopole dynamics in spin ice, J. Phys.: Condens. Matter **23**, 164222 (2011).

[42] G. Ehlers, A. L. Cornelius, T. Fennell, M. Koza, S. T. Bramwell, and J. S. Gardner, Evidence for two distinct spin relaxation mechanisms in 'hot' spin ice $Ho_2Ti_2O_7$, J. Phys.: Condens. Matter **16**, S635 (2004).

[43] S. T. Bramwell, M. N. Field, M. J. Harris, and I. P. Parkin, Bulk magnetization of the heavy rare earth titanate pyrochlores—A series of model frustrated magnets, J. Phys.: Condens. Matter **12**, 483 (2000).

[44] V. K. Anand, D. A. Tennant, and B. Lake, Investigations of the effect of nonmagnetic Ca substitution for magnetic Dy on spin-freezing in $Dy_2Ti_2O_7$, J. Phys.: Condens. Matter **27**, 436001 (2015).

[45] J. A. Paddison, H. Jacobsen, O. A. Petrenko, M. T. Fernández-Díaz, P. P. Deen, and A. L. Goodwin, Hidden order in spin-liquid $Gd_3Ga_5O_{12}$, Science **350**, 179 (2015).

[46] E. Bertaut and P. Burlet, Ordre magnetique a courte distance dans les solutions solides $Mn_xCr_{1-x}S$, Solid State Commun. **5**, 279 (1967).

[47] J. A. M. Paddison, J. R. Stewart, and A. L. Goodwin, Spinvert: A program for refinement of paramagnetic diffuse scattering data, J. Phys.: Condens. Matter **25**, 454220 (2013).

[48] J. A. M. Paddison and A. L. Goodwin, Empirical Magnetic Structure Solution of Frustrated Spin Systems, Phys. Rev. Lett. **108**, 017204 (2012).

[49] G. J. Nilsen, C. M. Thompson, G. Ehlers, C. A. Marjerrison, and J. E. Greedan, Diffuse magnetic neutron scattering in the highly frustrated double perovskite Ba_2YRuO_6, Phys. Rev. B **91**, 054415 (2015).

[50] J. A. M. Paddison, S. Agrestini, M. R. Lees, C. L. Fleck, P. P. Deen, A. L. Goodwin, J. R. Stewart, and O. A. Petrenko, Spin correlations in $Ca_3Co_2O_6$: Polarized-neutron diffraction and Monte Carlo study, Phys. Rev. B **90**, 014411 (2014).

[51] O. Arnold, O. Arnold, J. C. Bilheux, J. M. Borreguero, A. Buts, S. I. Campbell, L. Chapon, M. Doucet, N. Draper, R. Ferraz Leal, M. A. Gigg, V. E. Lynch, A. Markvardsen, D. J. Mikkelson, R. L. Mikkelson, R. Miller, K. Palmen, P. Parker, G. Passos, T. G. Perring, P. F. Peterson, S. Ren, M. A. Reuter, A. T. Savici, J. W. Taylor, R. J. Taylor, R. Tolchenov, W. Zhou, and J. Zikovsky, Mantid—Data analysis and visualization package for neutron scattering and μSR experiments, Nucl. Instrum. Methods Phys. Res. A **764**, 156 (2014).

[52] A. Yaouanc and P. Dalmas de Réotier, *Muon Spin Rotation, Relaxation, and Resonance: Applications to Condensed Matter* (Oxford University Press, Oxford, 2011).

[53] F. Bert, P. Mendels, A. Olariu, N. Blanchard, G. Collin, A. Amato, C. Baines, and A. D. Hillier, Direct Evidence for a Dynamical Ground State in the Highly Frustrated $Tb_2Sn_2O_7$ Pyrochlore, Phys. Rev. Lett. **97**, 117203 (2006).